Hindawi
Advances in Civil Engineering
Volume 2019, Article ID 7936513, 13 pages
https://doi.org/10.1155/2019/7936513

Research Article

Zoning Elastic Modulus Inversion for High Arch Dams Based on the PSOGSA-SVM Method

Bo Chen,[1,2,3] **Xiao Fu**,[1,2,3] **Xuyuan Guo**,[4] **Chongshi Gu**,[1,2,3] **Chenfei Shao**,[1,2,3] **and Xiangnan Qin**[1,2,3]

[1]*State Key Laboratory of Hydrology-Water Resources and Hydraulic Engineering, Hohai University, Nanjing 210098, China*
[2]*National Engineering Research Center of Water Resources Efficient Utilization and Engineering Safety, Hohai University, Nanjing 210098, China*
[3]*College of Water Conservancy and Hydropower Engineering, Hohai University, Nanjing 210098, China*
[4]*Yalong River Hydropower Development Company, Ltd., Chengdu 610051, China*

Correspondence should be addressed to Xiao Fu; fuxiaohhu@163.com and Chongshi Gu; csgu@hhu.edu.cn

Received 7 May 2019; Accepted 18 July 2019; Published 14 August 2019

Academic Editor: Emilio Bastidas-Arteaga

Real-time monitoring of the actual elastic modulus is essential and necessary to ensure the safe operation of arch dams. The zoning elastic modulus of a high arch dam is inversed by using deformation safety monitoring data in the operation period, based on the particle swarm optimization with gravitation search algorithm for support vector machine (PSOGSA-SVM) method. Firstly, the measured data of multipoints with a pendulum are separated to construct the initial sample training set; then, an optimal inversion model is established to reflect the complex nonlinear relationship between the mechanical parameters of the high arch dam and the deformation of measured points; finally, the PSOGSA-SVM method is used to train and dynamically update the training set so as to realize the optimization solution of the inversion model. The proposed inversion method is successfully applied to a high arch dam in China to verify its feasibility and validity. The results show that the actual elastic modulus of the dam body is much larger than the initial elastic modulus, which is beneficial to structural stability.

1. Introduction

China has built a large number of 300-meter-high concrete arch dams in the upper reaches of the Yangtze River and the Yellow River, such as Jinping-I of 305 m, Xiaowan of 294.5 m, Baihetan of 289 m, and Xiluodu of 285.5 m. These high dams and reservoirs are world-class projects, which can switch water disasters to water conservancy and provide the source power for national economic development. The topographic and geological conditions of the dam area are very complex. Determining the accurate physical and mechanical parameters of materials is the key to the structural deformation, stress, and stability of dams [1]. Therefore, in order to carry out the behavior diagnosis and rule analysis of a high arch dam during its operation period, it is urgent to study the method to accurately identify the real-time mechanical parameters.

Dam safety monitoring is a prototype test by 1 : 1. By using prototype observation data to carry out inversion analysis, the parameters most consistent with the actual working state of the project can be determined. According to the equation of finite element numerical simulation of concrete dams, the horizontal displacement of the dam crest is inversely proportional to the change of the dam body elastic modulus. Many scholars have carried out very meaningful research [2–14]. De Sortis and Paoliani [15] carried out the back analysis of the physical and mechanical parameters of a concrete buttress dam by establishing a mixed displacement model. Gu et al. [16] constructed the complex nonlinear relationship between relative values of hydraulic components of dam displacements and mechanical parameters for the roller-compacted concrete dam, by combining the partial least squares (PLS) regression and

least squares support vector machine (LSSVM) sample training method.

For the complex inversion analysis in practical engineering, the parameter inversion problem is often transformed into the optimization problem of the objective function. This process requires an efficient iterative method with strong nonlinear mapping capability and only a few samples. In recent years, such optimization methods have widely been developed [17–27], such as neural network method, confidence interval method, genetic algorithm, and particle swarm optimization. Liang et al. [28] comprehensively used artificial neural network and particle swarm optimization algorithm to invert the physical and mechanical parameters of the high and steep slope of the Dagangshan dam. Bui et al. [29] proposed a novel hybrid artificial intelligent approach, namely, swarm optimized neural fuzzy inference system, for modeling and forecasting the horizontal displacement of hydropower dams. Zhang et al. [30] considered the zone plans of rockfill dams based on the enhanced whale optimization.

This paper mainly focuses on the optimal inversion analysis of zoning elastic modulus of Jinping-I high arch dam in China. A reasonable statistical model is established to obtain the displacement components caused by water pressure. On this basis, the actual average elastic modulus of Jinping-I high arch dam is obtained by inversion. Finally, the real working strength of the arch dam is fed back through the simulation of the whole construction period. In the inversion analysis of the elastic modulus, considering the zoning characters, an effective PSOGSA-SVM method which can improve the speed and accuracy is established. This algorithm is simple, easy to implement, and fast to calculate when dealing with the extremum optimization problem. There is no requirement for the mathematical form of the objective function, and the gradient of the objective function, which is especially suitable for nonlinear and multiextremum optimization problems.

The inversion results show that the vertical deformation of Jinping-I high arch dam is relatively small, and the elastic modulus is increasing from now on, which is beneficial to structural stability. In other words, measured displacement of this high arch dam is much smaller than expected, which should arouse our attention. This phenomenon has not yet been unanimously explained by experts. What we need to do now is to strengthen safety monitoring and ensure the stable operation of Jinping-I high arch dam.

2. Inversion of Zoning Mechanics Parameters of High Arch Dams

2.1. Inversion Principle. In the initial stage of impoundment, the high arch dam has not experienced other sudden loads. The dam concrete is in the range of elastic deformation. The average elastic modulus and Poisson's ratio of the dam body and foundation are, respectively, E_c, μ_c, E_r and μ_r. The overall equilibrium equation of the three-dimensional finite element model of a high arch dam structure is as follows:

$$[K_0]\{\delta_0\} = \{R\}, \tag{1}$$

where $\{\delta_0\}$ is a nodal displacement array, $\{R\}$ is a nodal load array, and $[K_0]$ is a global stiffness matrix, which can be represented as

$$[K_0] = \sum_{e_j \in \Omega_c} [C]_{e_j}^{T} [k_0]_{e_j} [C]_{e_j} + \sum_{e_j \in \Omega_b} [C]_{e_j}^{T} [k_0]_{e_j} [C]_{e_j}, \tag{2}$$

$$\begin{aligned} [k_0]_{e_j} &= \iiint [B]^{T} \cdot [D_0] \cdot [B] d\Omega \\ &= E \iiint [B]^{T} \cdot f(\mu) \cdot [B] d\Omega = E\left[\overline{k}_0\right]_{e_j}, \end{aligned} \tag{3}$$

where $[k_0]_{e_j}$ is a unit stiffness matrix, $[C]_{e_j}$ is a transformation matrix between the node displacement of a unit and the displacement of the whole nodes, $[B]$ is a transformation matrix of strain, which is a constant matrix for a given unit, and $[D_0]$ is an elastic matrix, which is related to the elastic modulus and Poisson's ratio:

$$[D_0] = \frac{E}{(1+\mu)(1-2\mu)} \cdot \begin{bmatrix} 1-\mu & \mu & \mu & 0 & 0 & 0 \\ \mu & 1-\mu & \mu & 0 & 0 & 0 \\ \mu & \mu & 1-\mu & 0 & 0 & 0 \\ 0 & 0 & 0 & \frac{1-2\mu}{2} & 0 & 0 \\ 0 & 0 & 0 & 0 & \frac{1-2\mu}{2} & 0 \\ 0 & 0 & 0 & 0 & 0 & \frac{1-2\mu}{2} \end{bmatrix}. \tag{4}$$

Then equation (2) can be converted to

$$\begin{aligned} [K_0] &= E_c \sum_{e_j \in \Omega_c} [C]_{e_j}^{T} \left[\overline{k}_0\right]_{e_j} [C]_{e_j} + R \sum_{e_j \in \Omega_b} [C]_{e_j}^{T} \left[\overline{k}_0\right]_{e_j} [C]_{e_j} \\ &= E_c f\left(L, \mu_r, \mu_c, \frac{E_r}{E_c}\right) = E_c [\overline{K}_0], \end{aligned} \tag{5}$$

where $R = E_r/E_c$, L is the geometric size of the dam body, and $[K_0]$ is the ultimate stiffness of the structure.

Considering the short storage time, the influence of temperature load and aging factor can be neglected. The increment of external load is mainly caused by the change of reservoir water level. Therefore, the water pressure component δ_H is separated from the dam monitoring data, assuming the modulus of elasticity of the dam body and foundation are, respectively, E_{c0} and E_{r0}. The water pressure component $\delta_H'$is deduced by the structural analysis method.

At this time, the actual average elastic modulus of the dam body or foundation can be expressed as

$$E_c = E_{c0}\frac{\delta'_H}{\delta} \quad \text{or } E_r = E_{r0}\frac{\delta'_H}{\delta}. \tag{6}$$

Considering the zoning concrete characteristics of high arch dams, the increment of structural displacement under the uplift of reservoir water level is proportional to the elastic modulus combination of each zoning dam body and dam foundation.

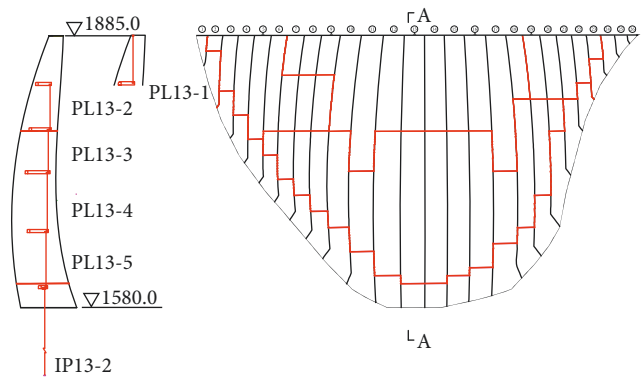

Figure 1: Layout of concrete zoning and pendulum of an arch dam.

2.2. Inversion Steps of Zoning Mechanics Parameters of a High Arch Dam. The measured vertical displacement of the high arch dam is the superimposed effect of deformation of dam concrete, dam foundation, and reservoir bedrock. In structural numerical simulation, the change of horizontal displacement of the arch dam is obviously affected by three zoning mechanical parameters. The inversion method of the dam body and dam foundation parameters, especially the joint inversion method by zoning multipoints, is studied in combination with zoning characters and pendulums of #13 dam section of a high arch dam.

The high arch dam body is divided into several concrete zones. Taking Jinping-I high arch dam as an example (Figure 1), in the area near the foundation surface of #3~#22 dam section and the area above 1778.00 m elevation in the dam section of river bed, Zone A concrete of $C_{180}40$ is used. In the area near the foundation surface of #1, #2, and #23~#26 dam sections on both sides and the area below 1778.00 m elevation in the river bed dam section, zone B concrete is $C_{180}35$. In the other areas above 1778.00 m elevation of both sides, zone C concrete is $C_{180}30$. Therefore, in view of the engineering problem, equation (2) is transformed into

$$[K_0] = \alpha E_A + \beta E_B + \gamma E_C, \tag{7}$$

where $\alpha = \sum_{e_j \in \Omega_A} [C]^T_{e_j} [\overline{k}_0]_{e_j} [C]_{e_j}$, $\beta = \sum_{e_j \in \Omega_B} [C]^T_{e_j} [\overline{k}_0]_{e_j} [C]_{e_j}$, and $\gamma = \sum_{e_j \in \Omega_C} [C]^T_{e_j} [\overline{k}_0]_{e_j} [C]_{e_j}$.

It can be concluded that the equations for calculating the elastic modulus inversion of high arch dams in different zones are as follows:

$$(E_A + aE_B + bE_C)\delta_H = (E_{A0} + aE_{B0} + bE_{C0})\delta'_H, \tag{8}$$

where E_{A0}, E_{B0}, and E_{C0} are, respectively, the assumed elastic modulus of zones A, B, and C; $a = \beta/\alpha$ and $b = \gamma/\alpha$.

The first inversion step of the high arch dam is to determine rock mechanics parameters of dam foundation by the inversion of vertical monitoring data. The inverted pendulums of a high arch dam foundation monitor the relative displacement from the deep suspension point to the buoy near the dam foundation. The inverted vertical suspension depth can reach about 100 m. When the inverted vertical suspension point is deep enough, it can be regarded as the absolute displacement of the dam foundation. Using displacement monitoring data of the inverted pendulum, the deformation modulus of dam foundation at the location of the inverted pendulum can be calculated by using equation (8).

The second inversion step of the high arch dam is to determine the mechanical parameters of dam zoning concrete by inversion of dam body monitoring data. Taking point A at dam crest as an example, the deformation under water pressure is composed of three parts: dam body deformation caused by water pressure δ_1, dam body deformation caused by rotation of dam foundation δ_2, and dam body deformation caused by shear of dam foundation δ_3. Figure 2 shows the deformation diagram of these three parts. In order to inverse dam body mechanics, it is necessary to separate the dam body deformation caused by the rotation of dam foundation and shear of dam foundation from the water pressure component δ_H of measured vertical data and the water pressure deformation δ'_H calculated by the finite element method. Then the first part of the dam body deformation required is obtained, and the mechanical parameters of the dam body can be inverted.

Therefore, equation (8) for inversion of dam body mechanical parameters can be transformed into the following equation:

$$(E_A + aE_B + bE_C)\delta_H = (E_{A0} + aE_{B0} + bE_{C0})\frac{\delta'_H - \delta'_2 - \delta'_3}{\delta_H - \delta_2}, \tag{9}$$

where δ'_H is the displacement of point A under water pressure with FEM under the assumption of the mechanical parameters and δ_H is the water pressure component of the displacement measured by the pendulum of point A separated by the monitoring model. δ'_2 and δ_2 are calculated displacement and measured displacement at point A caused by dam foundation corner, respectively. δ'_3 is the calculated displacement by FEM caused by dam foundation shear.

The measured displacement at point A caused by the turning angle of the dam foundation is the superposition of the upstream overhang of the arch dam caused by the action of reservoir water on the reservoir plate and the upstream tilt displacement of the arch dam caused by the action of reservoir water on the dam body. In order to simplify the calculation, the deformation from dam heel to dam toe caused by these two actions is assumed to be uniform. Generally speaking, this assumption can meet the

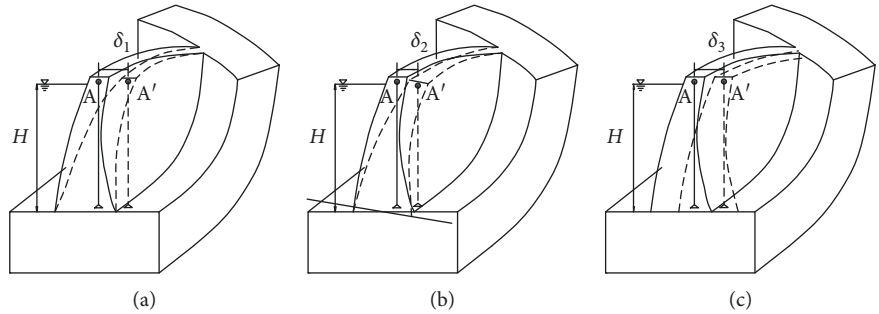

Figure 2: Three parts of the displacement component under water pressure.

requirements of engineering accuracy. Then the displacement component δ_2 of point A caused by the dam foundation turning angle can be expressed as

$$\delta_2 = h_{\mathrm{d}} \arctan \frac{v_{\mathrm{u}} - v_{\mathrm{d}}}{B}, \tag{10}$$

where h_{d} is the dam height of the calculation section and v_{u} and v_{d} are the vertical displacements of the dam heel and toe, respectively, which can be determined by the multipoint displacement meter of the dam heel and the displacement monitoring value of the dam toe.

There are many pendulums inside the high arch dam. The measured deformations of each pendulum can be expressed as δ_{ij}, where $i\,(i = 1, 2, \ldots, m)$ represents the dam section the pendulum is located and $j\,(j = 1, 2, \ldots, n)$ represents the vertical serial number calculated from the dam crest. The numerical results of relative deformation between two points corresponding to the vertical deformations are presented as δ'_{ij}.

Since the arch dam can self-adjust the stress state, it is necessary to further extract the pendulums which are sensitive to the elastic modulus of zoning dam concrete and to extract the relative displacement in the finite element model to improve the accuracy of the inversion results when using equation (9) to invert the elastic modulus of the high arch dam.

Sensitivity analysis of the pendulum system is determined by the finite element numerical simulation method. Firstly, the characteristic water levels $H_k\,(k = 1, 2, \ldots, l)$ corresponding to the storage steps of several high arch dams are selected, and then the relative displacement increment matrices $A_k = \left\{\delta'_{ijk}\right\}_{m\times n}$ of each pendulum under the action of each characteristic water level are calculated, respectively. Then, the displacement increment matrix $B_k = \left\{\delta'_{ijk}\right\}_{m\times n}$ of the j-th pendulum of i-th dam section under each characteristic water level is separated from the measured data. The sensitivity of the pendulum is determined by the similarity between the displacement increment matrices. The weight of each pendulum's contribution to the inversion is as follows:

$$\omega_{ij} = \frac{\left|\delta_{ijk} - \lambda\delta'_{ijk}\right|^{-1}}{\sum_{i=1}^{m}\sum_{j=1}^{n}\left|\delta_{ijk} - \lambda\delta'_{ijk}\right|^{-1}}, \tag{11}$$

where λ is determined by the minimum fitting error.

3. Multipoint Zoning Optimized Inversion Algorithms

3.1. Support Vector Regression-Based Multipoint Zoning Optimal Inversion Method. The inversion of the elastic modulus of high arch dams can be summarized as the following fitting optimization problems:

$$\mathrm{Var}\left[E_k(t)\right] = \min \sum_{i=1}^{m}\sum_{j=1}^{n} \omega_{ij}\left[\delta_{ij}(t) - \delta'_{ij}(t)\right]^2, \tag{12}$$

where E_k is the elastic modulus of each zoning concrete, including E_{A}, E_{B}, and E_{C}. m is the number of dam sections with the pendulum, and n is the number of pendulums. ω_{ij} is the weight of single measured point displacement. δ'_{ij} is the water pressure component with FEM, and δ_{ij} is the water pressure component with measured displacement, which can be obtained by the statistical model.

The support vector machine (SVM) [21, 22] is used to solve the above optimization problems between E_k and δ'_{ij}. Considering the nonlinear relationship between the displacement calculated by FEM and the elastic modulus of zoning concrete, $X_i\,(i = 1, 2, \ldots, n)$ is assumed as influencing factor set, which is the input sequence of each relative displacement calculation value. y_i is the input sequence of the inversion effects' value. Then, the distribution sample set $(X_i, Y_i)\,(i = 1, 2, \ldots, n)$ of the inversion of elastic modulus of concrete in high arch dams obeys the specific distribution $F(x, y)$ in function space $R^l \times R$, where $x \in R^l$ and $y \in R$. Then, using the idea of the support vector machine and nonlinear transformation $\phi(\cdot)$, the set of influencing factors is mapped from input space to high-dimensional feature space, and the optimal classification hyperplane function $f(x) = w^{\mathrm{T}} f(x) + b$ is found to fit the relationship between influencing factors X and effects y. The optimal support vector machine model of the inversion problem is obtained as

$$\begin{cases} \min \quad R(\mathbf{w}, \xi) = \dfrac{1}{2}\mathbf{w}^{\mathrm{T}}\mathbf{w} + C\sum_{i=1}^{n}\xi_i, \\ \qquad y_i\left[\mathbf{w}^{\mathrm{T}}\phi(x_i) + b\right] \geq 1, \\ \text{s.t} \quad \xi_i \geq 0, \\ \qquad i = 1, 2, \ldots, n, \end{cases} \tag{13}$$

where R denotes the risk function of the optimization problem. $\mathbf{w} = (w_1, w_2, \ldots, w_l)^{\mathrm{T}}$ is the weight vector of each influence factor. $C > 0$ is the penalty parameter, and x_i is the relaxation variable. $\sum \xi_i$ represents the deviation degree of effect monitoring data points from ideal classification conditions. $\phi(x)$ is a mapping function from input space to high-dimensional feature space, and b is a constant term reflecting bias.

According to the optimization theory and Wolfe duality technique [31, 32], the problem of minimizing the risk expectation of equation (13) is transformed into a duality problem. The Lagrange multiplier method is used to find the optimal solution at the saddle point of the function, and the insensitive loss function $L(y, f) = L(|y - f|_{\varepsilon})$ is defined to enhance the robustness and sparsity of the algorithm. The quadratic programming problem with the following inequality constraints is obtained:

$$\begin{cases} \max \quad -\varepsilon \sum_{i=1}^{n} (\alpha_i + \alpha_i^*) + \sum_{i=1}^{n} y_i (\alpha_i^* - \alpha_i) - \frac{1}{2} \sum_{i=1}^{n} \sum_{i=1}^{n} (\alpha_i^* - \alpha_i)\left[\alpha_j^* - \alpha_j\right] K\left(x_i - x_j\right), \\ \text{s.t.} \quad \sum_{i=1}^{n} (\alpha_i^* - \alpha_i) = 0, \quad \alpha_i, \alpha_i^* \in [0, C], \end{cases} \tag{14}$$

where $\alpha = \{\alpha_1, \alpha_2, \ldots, \alpha_n\}^{\mathrm{T}}$ denotes the Lagrange multipliers; $f(x_i)$ and $f(x_j)$ are the nonlinear transformation function; $\alpha_i^* (i = 1, 2, \ldots, n)$ is the Lagrange multiplier corresponding to α_i and $\alpha_i^* \alpha_i = 0$; and only if $\alpha_i^* \neq \alpha_i$, the corresponding data sample points are defined as support vectors.

The idea of solving the abovementioned nonlinear problems is to map the low-dimensional input samples into the high-dimensional space by introducing the kernel function and transform the nonlinear support vector regression into a linear problem so as to construct the optimal hyperplane solution. According to functional theory, the inner product function $K(x_i, x_j)$ satisfying Mercer condition $K(x_i, x_j) = f(x_i) f(x_j)$ is the kernel function to be sought. In this paper, the radial basis function (RBF) kernel function is used to solve the problem, which can be expressed as

$$K\left(x_i, x_j\right) = \exp\left(\frac{-\left|x_i - x_j\right|^2}{2\sigma^2}\right). \tag{15}$$

3.2. Particle Swarm Optimization with Gravitation Search Algorithm for Support Vector Machine Modeling Parameters. The key to obtain the optimal solution of equation (13) is to select the appropriate radical basis function width σ and penalty parameters C. A particle swarm optimization with gravitation search algorithm (GSA) [33, 34] is introduced here to approximate the optimal solution of the two parameters. The corresponding solutions of σ and C are regarded as a group of particles moving in the solution space, and the optimization degree of the solution is regarded as the mass of the particles. In the solution, the particles are expected to follow the spatial kinematics law and move towards the position with the highest mass. In each iteration, the position, velocity, and acceleration of the particle movement are updated, i.e.,

$$\begin{aligned} x_i^d(k+1) &= x_i^d(k) + v_i^d(k+1), \\ v_i^d(k+1) &= v_i^d(k) + a_i^d(k), \\ a_i^d &= \frac{F_i^d(k)}{M_i(k)}, \\ F_i^d(k) &= \sum_{j \in N, i \neq j} \frac{G_0 \times M_i(k) \times M_j(k)}{\left(x_i^d(k) - x_j^d(k)\right)^2}, \end{aligned} \tag{16}$$

where $x_i^d(k)$, $v_i^d(k)$, and $a_i^d(k)$ denote the position, velocity, and acceleration of the k-th generation particles i in the d-th dimensional space, respectively and G_0 is the iterated gravitational constant.

In order to consider the memory of particles, the idea of particle evolutionary computation in particle swarm optimization (PSO) is introduced to improve the iteration speed. Then, the velocity update equation is transformed into

$$\begin{aligned} v_i^d(k+1) = \omega v_i^d(k) &+ c_1 \times r \times \left(x_i^d(\text{best}) - x_i^d(k)\right) \\ &+ c_2 \times r \times \left(x_g^d(\text{best}) - x_i^d(k)\right), \end{aligned} \tag{17}$$

where ω denotes the inertia factors; c_1 and c_2 represent the acceleration factors; $x_i^d(\text{best})$ is the individual optimal position of particle i during k iteration process; and $x_g^d(\text{best})$ is the global optimal position of all the particles during k iteration process.

3.3. Realization of Optimized Inversion of Multipoint Zoning Concrete of High Arch Dams. In the optimized inversion of the multipoint zoning concrete method, based on the construction of the initial sample training set, the set is updated dynamically and continuously trained to establish the optimal inversion model which can reflect the complex nonlinear relationship between the elastic modulus of the zoning concrete and the displacement of the measured

points. The elastic modulus of zoning concrete of the high arch dam can be inverted by inputting the measured displacement of the separated measured points. Its main implementation process is shown in Figure 3. The main steps are as follows:

Step 1. Establish the safety monitoring model between measured displacement and environmental factors of the pendulum system, separate the water pressure component, and separate the displacement caused by the deformation of reservoir plate and the shear of dam foundation further.

Step 2. Considering engineering materials and structural zone of the dam body concrete, dam foundation rock, replacement body, cracks, faults, and weak structural surfaces, establish a three-dimensional finite element model of the arch dam.

Step 3. Determine the elastic modulus parameter groups of E_A, E_B, E_C, and E_D and their respective ranges according to the material characteristics of zoning dam concrete, and then construct the parameter combinations to be inverted by the orthogonal experimental design method.

Step 4. Separate the displacement values calculated by FEM corresponding to each pendulum, carry out sensitivity analysis, determine the contribution of each pendulum to the inversion, and then select the main contributing factors to construct the training sample set and test sample set of SVM regression modeling.

Step 5. Load the radial basis function parameter σ and penalty parameter C of the SVM model on the individual space particles, use the particle swarm optimization with gravitation search algorithm method to iterate the optimal spatial position of the individual particle, and decompose the particle to obtain the optimal parameters of the SVM regression model.

Step 6. Load the parameters to be inverted E_A, E_B, E_C, and E_D onto the individual space particles, use the particle swarm gravitation search algorithm to iterate the optimal spatial position of the individual particles, and then decompose the particles to obtain the optimal parameters to be inverted.

4. Case Study

The Jinping-I high arch dam is located in southwest China, which is mainly used for power generation and flood control of the Yalong River. Its layout chart is shown in Figure 4. The normal water level is 1880.0 m with the storage capacity below 7.8×10^9 m^3. The dam crest elevation is 1885.0 m, and the minimum foundation surface elevation is 1580.0 m. The maximum dam height is 305.0 m, which means it is the highest arch dam in the world. The width of the dam crest is 16.0 m, the thickness of the dam bottom is 63.0 m, and the ratio of thickness to height is 0.207.

4.1. Selection of Inversion Data. In the dam monitoring system, the pendulum can directly reflect the dam deformation with high accuracy. The measured data show that the radial deformation of the middle part of the dam is obviously affected by water pressure and is less restricted by the mountains on both sides of the river. Therefore, 24 measured points in sections #5, #9, #11, #13, #16, and #19 are taken as calculation data in the process of inversion. According to the installation drawings of the pendulum system, the corresponding notes of the finite element model are processed by accumulating and transforming the X and Y directions data into tangential and radial data. Then, the model parameters are inverted by comparing with the measured values. Figure 5 is the pendulum system of some main dam sections.

Figure 6 shows the measured radial displacement increment nephogram of the arch dam from the water level of 1808.14 m on June 1, 2017, to that of 1878.16 m on December 31, 2018. Figure 7 shows the measured tangential displacement increment nephogram during this period.

From the radial displacement and tangential displacement increment nephograms of the pendulum system, it can be seen that the overall zoning rule of radial displacement is obvious. In addition, the increment value of radial displacement is large, which can be taken as the main basis for inversion. Figure 8 shows the fitting water pressure component δ_H, temperature component δ_T, and aging component δ_θ of the radial displacement of measured point PL13-3 in dam section #13 with the stepwise regression algorithm. It can be seen that the radial displacement of measured point is mainly affected by water pressure. Therefore, the water pressure component of radial displacement of the pendulum system is selected for inversion.

4.2. FEM Simulation. Based on engineering design and geological data, a three-dimensional finite element model of the high arch dam is established to study dam working state. The finite element is built according to the two-dimensional engineering drawings, and the simulation calculation is conducted with the finite element software. Figures 9 and 10 show the finite element model which consists of 923737 elements and 957221 nodes, and the number of nodes and elements for dam body is 36079 and 29840, respectively. The mesh for the dam body and foundation are relatively fine and coarse by progressive meshing technique to achieve a balance between accuracy and efficiency of the simulation. Furthermore, several models with different element sizes were established for mesh validation, which demonstrated that the selected model satisfies the demand calculation accuracy. Hexahedral eight-node isoparametric element is mainly used in the finite element model. Also, pentahedral six-node isoparametric element is used in some areas considering the topographic and geological effects. The main weak structural surfaces, such as f2, f5, f8, f42-9, f13, f14, and f18 faults, are simulated during the meshing of foundation. In addition, topographic, stratigraphic zoning and some engineering measures such as concrete cushion, concrete plug, shear transferring tunnel, second dam, plunge pool,

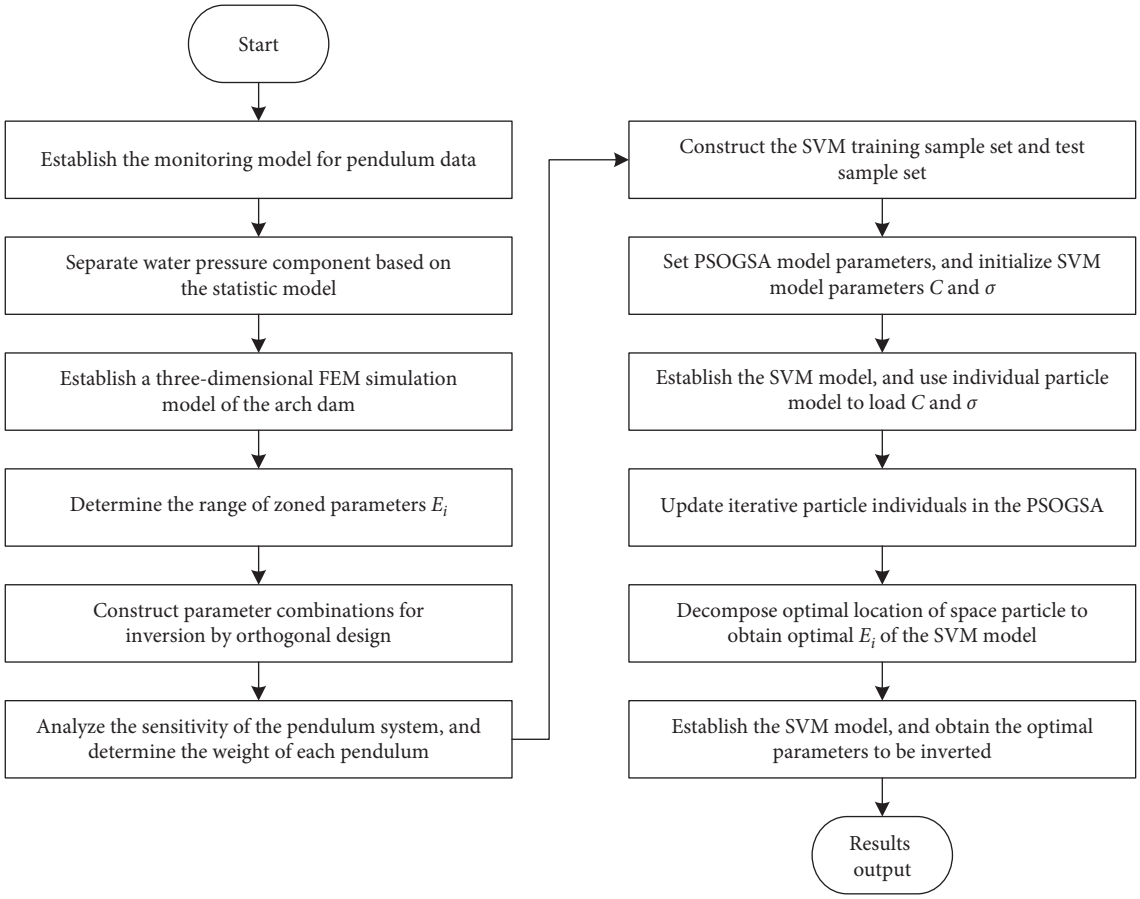

Figure 3: PSOGSA-SVM inversion process of zoning high arch dams.

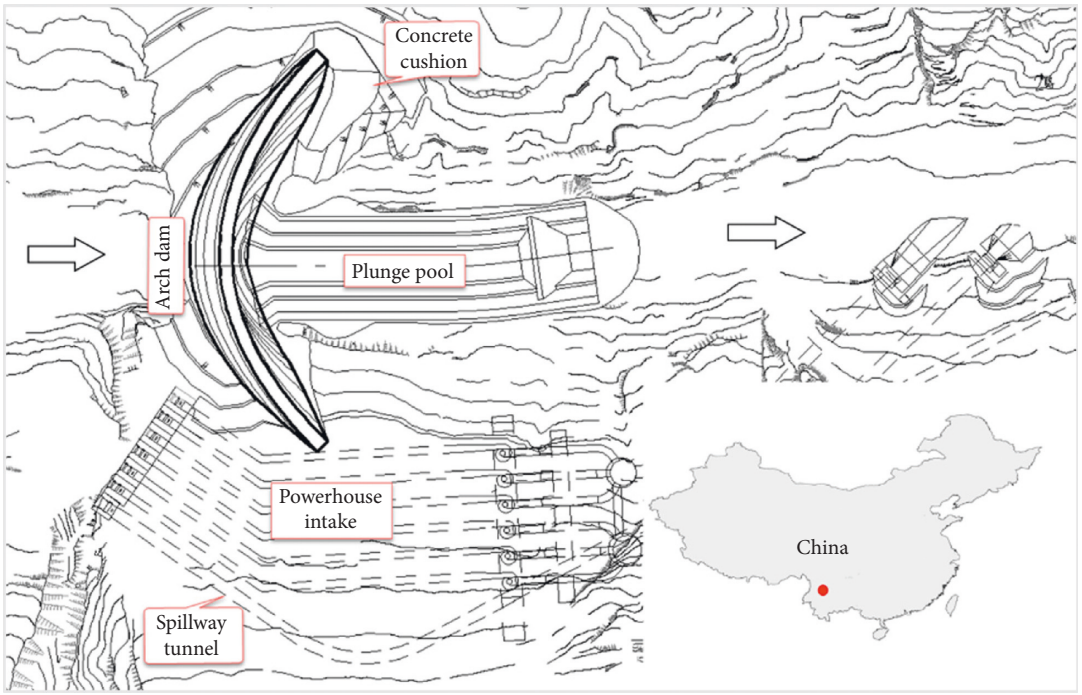

Figure 4: Layout chart of the Jinping-I high arch dam.

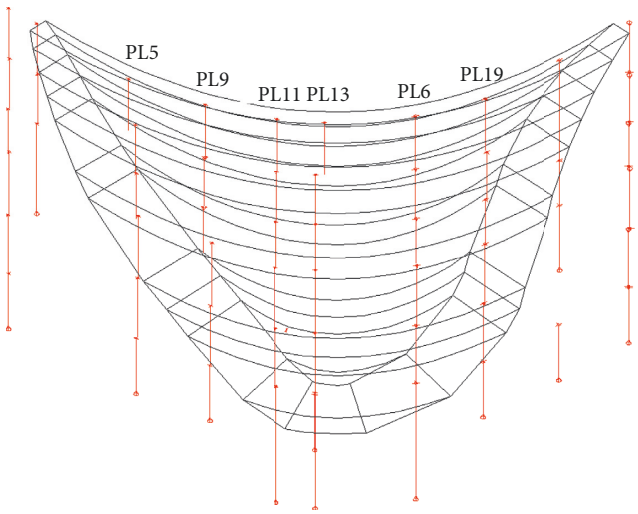

Figure 5: Pendulum system of some main dam sections.

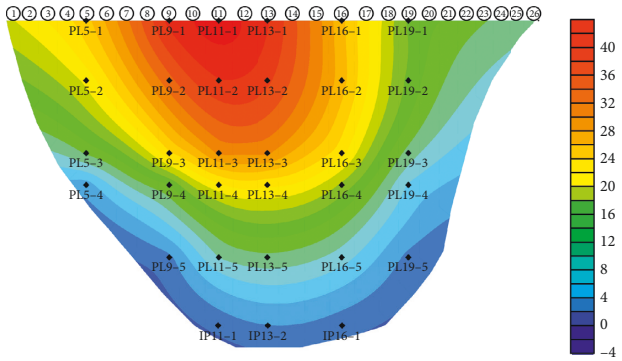

Figure 6: Radial displacement increment nephogram (to the downstream is positive).

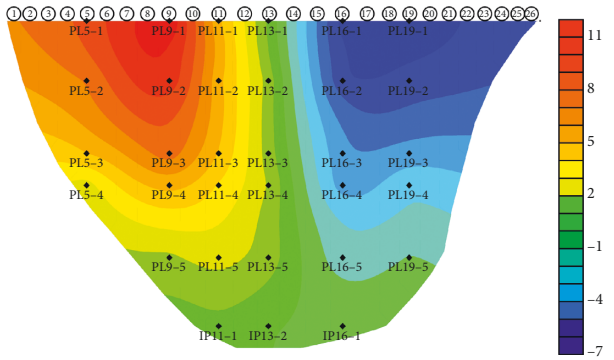

Figure 7: Tangential displacement increment nephogram (to the left bank is positive).

and grouting treatment are simulated. Figure 11 shows the zoning concrete of the dam body model. The high arch dam body is divided into zone A, zone B, and zone C according to the construction manual.

Selection of the coordinate system in the model: X-axis is perpendicular to the arch dam center line, pointing to the left bank is positive (SE62°); Y-axis is parallel to the arch dam center line, pointing downstream is positive (NE28°); and Z-axis is positive in the vertical upward direction.

4.3. Inverse Modeling Analysis Procedure. The geological conditions of the dam foundation and the mountain body on both sides of the river are complex, and the rock mass parameters of each part are different, which have little influence on the calculation value of the dam deformation. Therefore, the simplified calculation regards the dam foundation and the mountain body on both sides of the river as a whole, that is, the dam foundation and the mountain body on both sides of the river are regarded as zone D, with a comprehensive elastic modulus parameter E_D.

For the inversion range of elastic modulus of A, B, C, and D zones, consulting the research papers of relevant scholars, the elastic modulus of the Jinping-I high arch dam body and dam foundation are usually larger than the initial elastic modulus. In addition, considering that A, B, and C zones concrete in dam construction is $C_{180}40$, $C_{180}35$, and $C_{180}30$, respectively, with the initial modulus of 24.0 GPa, 23.5 GPa, and 23.0 GPa. The difference is little, so the first assumption is that the dam body is homogenous, and the range is $E_A = E_B = E_C \in [30\,\text{GPa}, 48\,\text{GPa}]$. Considering the content of construction report, the elastic modulus range of dam foundation is estimated as $E_D \in [24\,\text{GPa}, 39\,\text{GPa}]$. It should be noted that the elastic modulus inversion of the homogeneous dam body is only a rough inversion of the elastic modulus range of the dam body and foundation, which provides a basis for the next accurate inversion.

We select the statistical model of the stepwise regression algorithm to preprocess the inversion data and select δ_H, δ_T, and δ_θ as components.

The water pressure component of pendulum radial displacement increment from June 1, 2017, to December 31, 2018, is extracted on the basis of finite element simulation inversion.

The separation results of pendulum radial displacement increment of some main measuring points are as follows by using statistical model. δ is the measured value of the radial deformation, δ_H is the water pressure component, δ_T is the temperature component, δ_θ is the aging component, and ε is the error between the measured value and the sum of three components above.

From Table 1 and Figure 12, we can see that the error of the statistical model of the stepwise regression algorithm is small, which means that the separation result is credible and the water pressure component used for the finite element analysis is reasonable as well.

Based on assumption that the dam body is homogenous and dam foundation is simplified, which means $E_A = E_B = E_C \in [30\,\text{GPa}, 48\,\text{GPa}]$ and $E_D \in [24\,\text{GPa}, 39\,\text{GPa}]$. The dam body and dam foundation elastic modulus ranges are, respectively, substituted into the finite element model with the increment of 3 GPa. In other words, $E_A = E_B = E_C \in$ (30 GPa, 33 GPa, 36 GPa, 39 GPa, 42 GPa, 45 GPa, 48 GPa), and $E_D \in [24\,\text{GPa}, 27\,\text{GPa}, 30\,\text{GPa}, 33\,\text{GPa}, 36\,\text{GPa}, 39\,\text{GPa}]$. The number of combined results is $7 \times 6 = 42$.

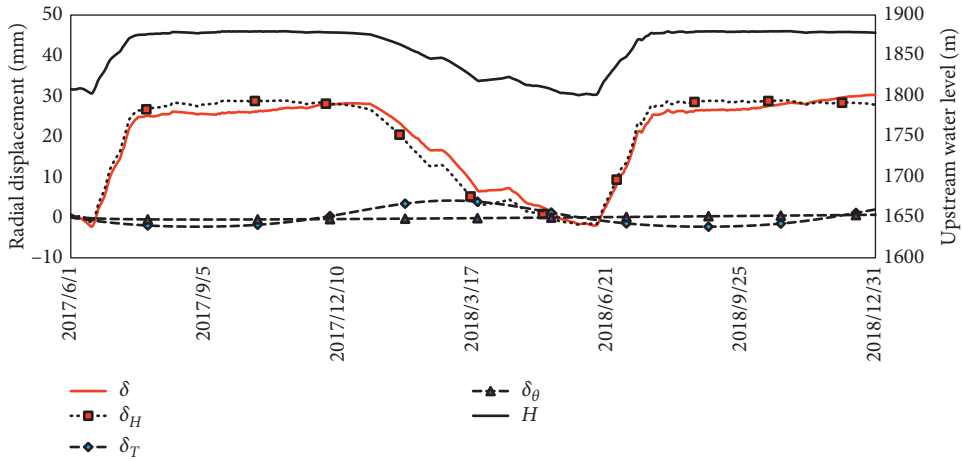

Figure 8: Fitting components of radial displacement of PL13-3.

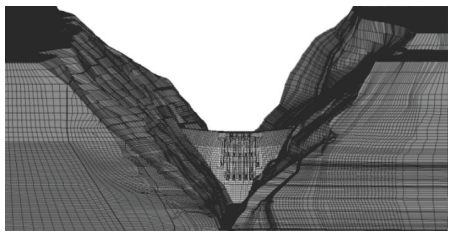

Figure 9: Three-dimensional finite element model of the Jinping-I arch dam (upstream viewpoint).

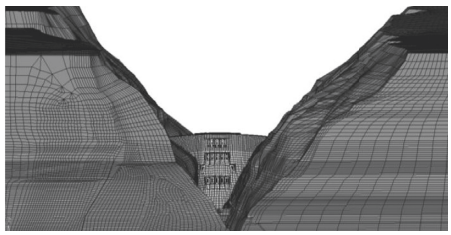

Figure 10: Three-dimensional finite element model of the Jinping-I arch dam (downstream viewpoint).

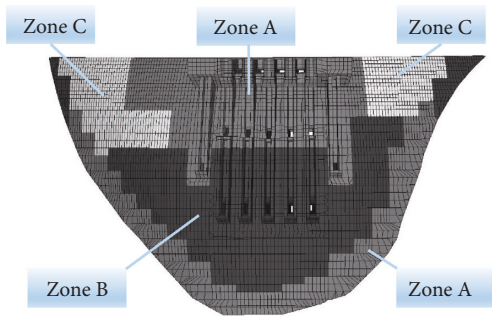

Figure 11: Finite element model of zoning concrete of the dam body.

The incremental value δ_{Hc} of water pressure component of radial displacement deformation of 42 groups of 24 measuring points is calculated. The standard deviation σ

Table 1: Separation results of pendulum radial displacement increment.

Points	δ	δ_H	δ_T	δ_θ	ε
PL5-2	20.54	16.26	16.26	3.40	0.19
PL5-3	12.35	9.82	9.82	1.49	0.13
PL5-4	4.79	3.06	3.06	0.78	0.04
PL9-3	23.65	21.49	21.49	1.86	0.01
PL9-4	13.81	12.85	12.85	0.67	−0.02
PL9-5	3.43	3.20	3.20	0.14	−0.02
PL11-2	37.90	33.46	33.46	4.24	−0.01
PL11-3	30.47	27.69	27.69	2.15	−0.10
PL11-4	21.52	19.68	19.68	1.04	−0.15
PL11-5	10.06	9.02	9.02	0.30	−0.10
IP11-1	2.65	2.24	2.24	0.02	−0.03
PL13-3	30.38	27.89	27.89	1.94	0.09
PL13-4	22.33	20.93	20.93	0.83	−0.01
PL13-5	11.49	10.73	10.73	0.23	0.06
IP13-2	3.94	3.04	3.04	0.05	0.13
PL16-2	26.94	22.69	22.69	2.59	0.13
PL16-3	22.88	19.69	19.69	0.91	0.02
PL16-4	17.52	14.90	14.90	0.28	−0.04
PL16-5	8.96	7.83	7.83	0.29	0.01
IP16-1	2.83	2.15	2.15	0.08	0.03
PL19-2	15.43	11.23	11.23	2.66	−0.27
PL19-3	11.18	8.59	8.59	1.22	0.06
PL19-4	7.70	6.12	6.12	0.43	−0.02
PL19-5	3.43	2.23	2.23	0.20	0.03

between the water pressure component extracted increment from 24 measuring points and that calculated from the finite element model is chosen as the objective function:

$$f(E_A, E_D) = \sigma = \sqrt{\sum_{i=1}^{24} (\delta_{iH} - \delta_{iHc})^2}. \quad (18)$$

When the value of σ is the smallest, it shows that the elastic modulus simulated is the closest to the actual elastic modulus. The calculation results are shown in Table 2.

From Table 2 and Figure 13, we can estimate that the elastic modulus distribution which is closest to the actual

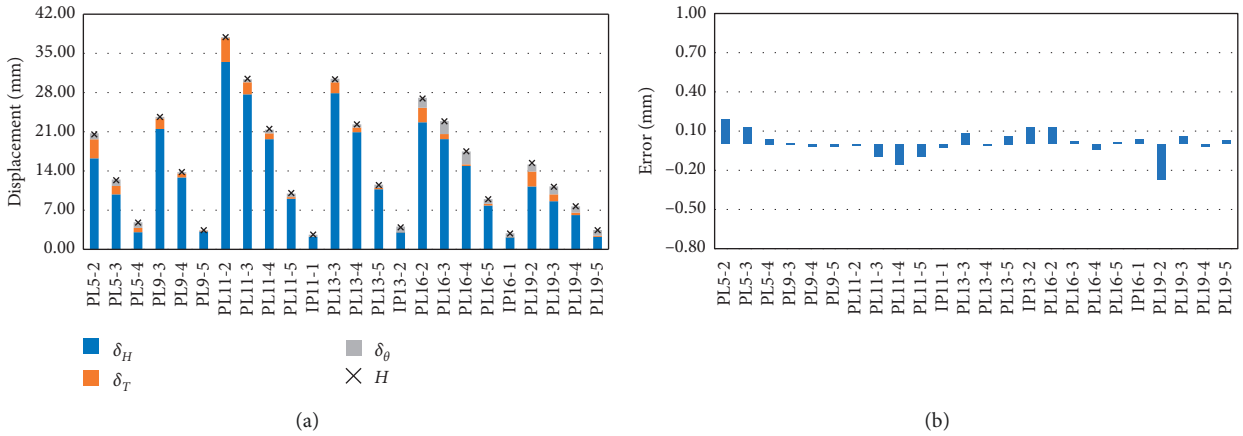

Figure 12: Separation results of pendulum radial displacement increment.

Table 2: Standard deviations of the combined results of E_A and E_D.

E_D	$E_A = E_B = E_C$						
	30 GPa	33 GPa	36 GPa	39 GPa	42 GPa	**45 GPa**	48 GPa
24 GPa	30.59	22.97	16.67	11.43	7.22	4.49	4.46
27 GPa	27.89	20.34	14.11	9.03	5.29	**4.13**	5.91
30 GPa	25.73	18.24	12.11	7.27	4.38	5.03	7.60
33 GPa	23.96	16.53	10.53	6.05	4.39	6.28	9.16
36 GPa	22.49	15.13	9.29	5.32	4.98	7.52	10.54
39 GPa	21.24	13.97	8.32	5.01	5.77	8.66	11.75

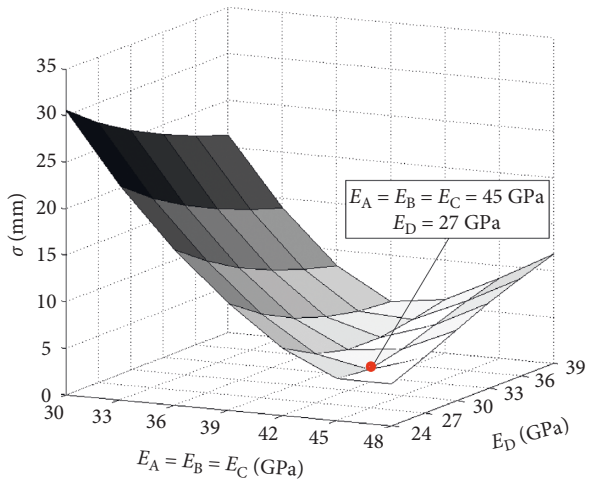

Figure 13: Three-dimensional graph of standard deviation of combined results of E_A and E_D.

Table 3: Assumed elastic modulus range of A, B, C, and D zones (GPa).

	E_A	E_B	E_C	E_D
Homogeneous value	45.0	45.0	45.0	45.0
Range of actual value	44.0–46.0	43.5–45.5	43.0–45.0	26.0–28.0

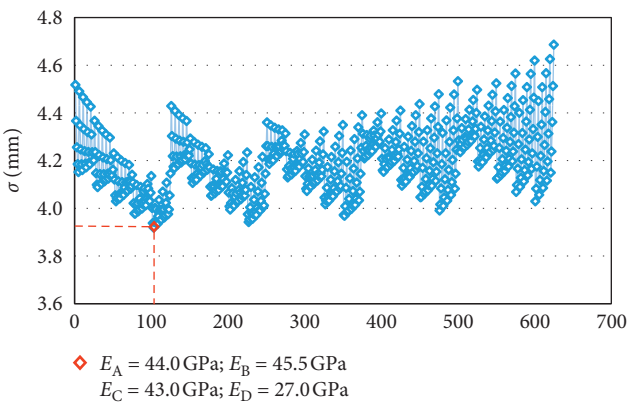

Figure 14: Standard deviation of combined results of E_A E_B E_C, and E_D with the PSOGSA-SVM algorithm.

elastic modulus is that $E_A = E_B = E_C = 45$ GPa and $E_D = 27$ GPa if we assume that the dam body is homogeneous.

Next, considering the zoning of the dam body, the assumed elastic modulus range of A, B, C, and D zones are as shown in Table 3.

The PSOGSA-SVM algorithm described above is used to construct training samples set and testing samples set. The results are as follows.

From Figure 14, we can see that when $E_A = 44.0$ GPa, $E_B = 45.5$ GPa, $E_C = 43.5$ GPa, and $E_D = 27.0$ GPa, the standard deviation is smallest, which means the calculated elastic modulus is the closest to the actual value.

Figure 15 shows the comparison of the water pressure component δ_{HC} of the calculated elastic modulus and the measured value δ_{HM} of the statistical model mentioned above.

Then, we take the inversion results into the calculation of the pendulum system. The comparison nephograms between the calculated radial displacement and tangential displacement and those of the measured are as follows.

From Figures 16 and 17, the difference between the calculated displacement of inverted parameters and the measured displacement, which means the inversion results, is reasonable and credible.

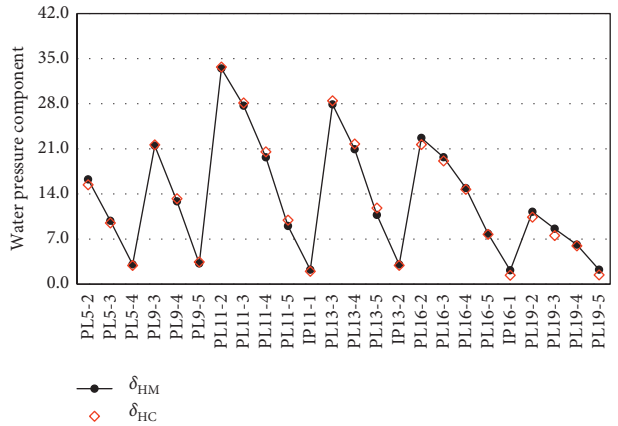

Figure 15: Water pressure component δ_{HC} of the calculated elastic modulus and the measured value δ_{HM} of the statistical model.

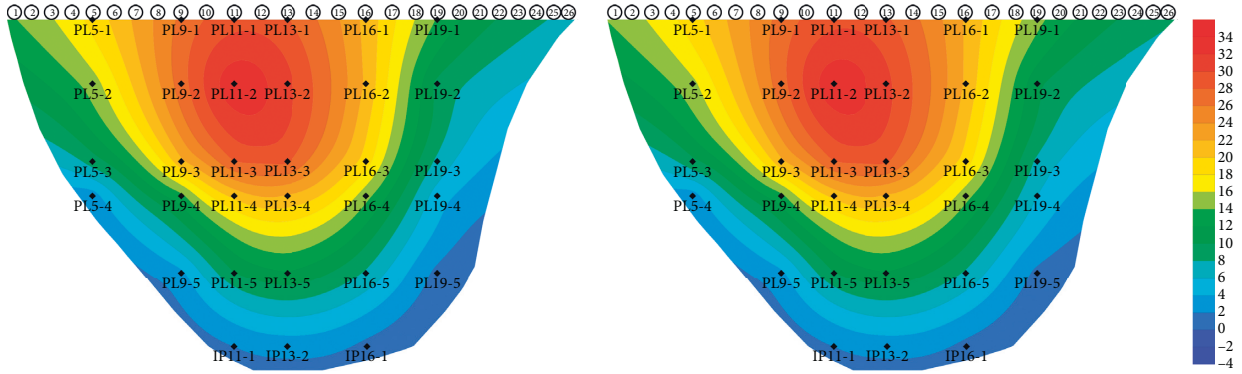

Figure 16: Comparison nephogram between the calculated radial displacement and that of the measured.

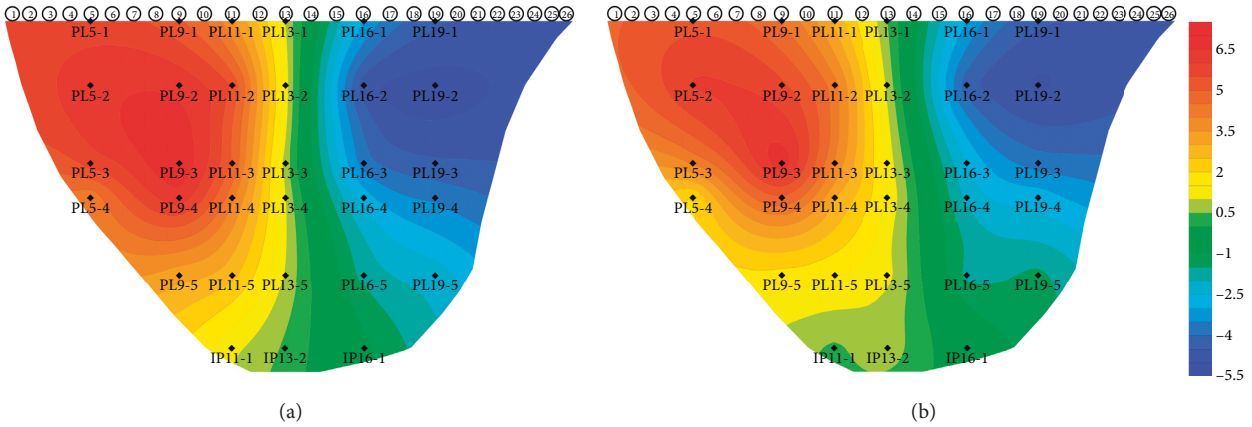

Figure 17: Comparison nephogram between the calculated tangential displacement and that of the measured.

5. Conclusion

An optimal analysis method has been proposed to invert the zoning elastic modulus of the Jinping-I high arch dam. The water pressure component of radial displacement of main measured points is obtained with the statistic model as the calibration. A new PSOGSA-SVM optimization method is carried out to solve the inversion problem, which is of great significance to improve the efficiency and accuracy. The results are reasonable and reliable.

Considering with the similar studies of other scholars, the results of $E_A = 44.0$ GPa, $E_B = 45.5$ GPa, $E_C = 43.5$ GPa,

and $E_D = 27.0$ GPa show that the real elastic modulus of the dam body is much larger than the initial elastic modulus and it is increasing in recent years. It shows that the displacement of the Jinping-I high arch dam is smaller than expected, which means it is beneficial to structural stability. However, it should be mentioned that it is possible that some unknown reasons that cause the dam displacement smaller deserves much more attention in many aspects. It is necessary to strengthen safety monitoring and ensure the stable operation of the Jinping-I high arch dam.

Data Availability

The data used to support the findings of this study are available from the corresponding author upon request.

Conflicts of Interest

The authors declare that there are no conflicts of interest.

Acknowledgments

This work was supported by the National Key R&D Program of China (Grant no. 2016YFC0401908), National Natural Science Foundation of China (Grant nos. 51739003, 51579085, 51779086, 51579086, 51379068, 51579083, and 51609074), project funded by the Priority Academic Program Development of Jiangsu Higher Education Institutions (YS11001), special project funded by the National Key Laboratory (20165042112), and Key R&D Program of Guangxi (AB17195074).

References

[1] B. Sevim, A. C. Altunişik, A. Bayraktar, M. Akköse, and S. Adanur, "Estimation of elasticity modulus of a prototype arch dam using experimental methods," *Journal of Materials in Civil Engineering*, vol. 24, no. 4, pp. 321–329, 2012.

[2] P. Bonaldi, M. Fanelli, and G. Guiseppetti, "Displacement forecasting for concrete dams," *International Water Power and Dam Construction*, vol. 29, no. 9, pp. 42–50, 1977.

[3] Z. Wei, C. Xiaolin, Z. Chuangbing, and L. Xinghong, "Failure analysis of high-concrete gravity dam based on strength reserve factor method," *Computers and Geotechnics*, vol. 35, no. 4, pp. 627–636, 2008.

[4] S. R. Oro, T. R. Mafioleti, A. C. Neto, S. R. P. Garcia, and C. N. Júnior, "Study of the influence of temperature and water level of the reservoir about the displacement of a concrete dam," *International Journal of Applied Mechanics and Engineering*, vol. 21, no. 1, pp. 107–120, 2016.

[5] B. Sevim, A. Bayraktar, and A. C. Altunisik, "Investigation of water length effects on the modal behavior of a prototype arch dam using operational and analytical modal analyses," *Structural Engineering and Mechanics*, vol. 37, no. 6, pp. 593–615, 2011.

[6] S. Pereira, F. Magalhães, J. P. Gomes, Á. Cunha, and J. V. Lemos, "Dynamic monitoring of a concrete arch dam during the first filling of the reservoir," *Engineering Structures*, vol. 174, pp. 548–560, 2018.

[7] J. Mata, A. T. de Castro, and J. S. da Costa, "Constructing statistical models for arch dam deformation," *Structural Control and Health Monitoring*, vol. 21, no. 3, pp. 423–437, 2014.

[8] X. Fu, C. Gu, and D. Qin, "Deformation features of a super-high arch dam structural system," *Optik*, vol. 130, pp. 681–695, 2017.

[9] F. Li, Z. Wang, and G. Liu, "Towards an error correction model for dam monitoring data analysis based on cointegration theory," *Structural Safety*, vol. 43, pp. 12–20, 2013.

[10] H. Su, X. Li, B. Yang, and Z. Wen, "Wavelet support vector machine-based prediction model of dam deformation," *Mechanical Systems and Signal Processing*, vol. 110, pp. 412–427, 2018.

[11] B. Sevim, "The effect of material properties on the seismic performance of arch dams," *Natural Hazards and Earth System Sciences*, vol. 11, no. 8, pp. 2253–2261, 2011.

[12] D. J. Zheng, X. Q. Li, M. Yang, H. Z. Su, and C. S. Gu, "Copula entropy and information diffusion theory-based new prediction method for high dam monitoring," *Earthquake Structure*, vol. 14, no. 2, pp. 143–153, 2018.

[13] B. Sevim, A. Bayraktar, A. C. Altunışık, S. Adanur, and M. Akköse, "Dynamic characteristics of a prototype arch dam," *Experimental Mechanics*, vol. 51, no. 5, pp. 787–791, 2011.

[14] X. Fu, C. Gu, X. Zheng, H. Su, and X. Qin, "Kriging risk model of dam failure based on HL-RF algorithm," *Fresenius Environmental Bulletin*, vol. 27, no. 5, pp. 3409–3418, 2018.

[15] A. De Sortis and P. Paoliani, "Statistical analysis and structural identification in concrete dam monitoring," *Engineering Structures*, vol. 29, no. 1, pp. 110–120, 2007.

[16] C. Gu, B. Li, G. Xu, and H. Yu, "Back analysis of mechanical parameters of roller compacted concrete dam," *Science China Technological Sciences*, vol. 53, no. 3, pp. 848–853, 2010.

[17] R. Fedele, G. Maier, and B. Miller, "Health assessment of concrete dams by overall inverse analyses and neural networks," *International Journal of Fracture*, vol. 137, no. 1–4, pp. 151–172, 2006.

[18] B. Sevim, A. C. Altunisik, and A. Bayraktar, "Experimental evaluation of crack effects on the dynamic characteristics of a prototype arch dam using ambient vibration tests," *Computers & Concrete*, vol. 10, no. 3, pp. 277–294, 2012.

[19] R. Ardito, P. Bartalotta, L. Ceriani, and G. Maier, "Diagnostic inverse analysis of concrete dams with statical excitation," *Journal of the Mechanical Behavior of Materials*, vol. 15, no. 6, pp. 381–390, 2004.

[20] I. Karimi, N. Khaji, M. T. Ahmadi, and M. Mirzayee, "System identification of concrete gravity dams using artificial neural networks based on a hybrid finite element-boundary element approach," *Engineering Structures*, vol. 32, no. 11, pp. 3583–3591, 2010.

[21] J. Y. Liu and H. Z. Liu, "Arch dam deformation prediction model based on PSO-SVM," *Applied Mechanics and Materials*, vol. 351-352, pp. 1306–1311, 2013.

[22] M. Babaei, R. Moeini, and E. Ehsanzadeh, "Artificial neural network and support vector machine models for inflow prediction of dam reservoir (case study: Zayandehroud dam reservoir)," *Water Resources Management*, vol. 33, no. 6, pp. 2203–2218, 2019.

[23] B. Stojanovic, M. Milivojevic, N. Milivojevic, and D. Antonijevic, "A self-tuning system for dam behavior modeling based on evolving artificial neural networks," *Advances in Engineering Software*, vol. 97, pp. 85–95, 2016.

[24] B. Ahmadi-Nedushan, "Prediction of elastic modulus of normal and high strength concrete using ANFIS and optimal nonlinear regression models," *Construction and Building Materials*, vol. 36, pp. 665–673, 2012.

[25] H. Gu, Z. Wu, X. Huang, and J. Song, "Zoning modulus inversion method for concrete dams based on chaos genetic optimization algorithm," *Mathematical Problems in Engineering*, vol. 2015, Article ID 817241, 9 pages, 2015.

[26] B. Chen, C. Gu, T. Bao, B. Wu, and H. Su, "Failure analysis method of concrete arch dam based on elastic strain energy criterion," *Engineering Failure Analysis*, vol. 60, pp. 363–373, 2016.

[27] D. Zheng, L. Cheng, T. Bao, and B. Lv, "Integrated parameter inversion analysis method of a CFRD based on multi-output support vector machines and the clonal selection algorithm," *Computers and Geotechnics*, vol. 47, pp. 68–77, 2013.

[28] Z. Liang, B. Gong, C. Tang, Y. Zhang, and T. Ma, "Displacement back analysis for a high slope of the Dagangshan hydroelectric power station based on BP neural network and particle swarm optimization," *The Scientific World Journal*, vol. 2014, Article ID 741323, 11 pages, 2014.

[29] K.-T. T. Bui, D. Tien Bui, J. Zou, C. Van Doan, and I. Revhaug, "A novel hybrid artificial intelligent approach based on neural fuzzy inference model and particle swarm optimization for horizontal displacement modeling of hydropower dam," *Neural Computing and Applications*, vol. 29, no. 12, pp. 1495–1506, 2018.

[30] J. Zhang, D. Zhong, M. Zhao, J. Yu, and F. Lv, "An optimization model for construction stage and zone plans of rockfill dams based on the enhanced whale optimization algorithm," *Energies*, vol. 12, no. 3, p. 466, 2019.

[31] F. Giannessi and G. Mastroeni, "Separation of sets and wolfe duality," *Journal of Global Optimization*, vol. 42, no. 3, pp. 401–412, 2008.

[32] H. C. Wu, "Wolfe duality for interval-valued optimization," *Journal of Optimization Theory and Applications*, vol. 138, no. 3, pp. 497–509, 2008.

[33] D. Hu, A. Sarosh, and Y.-F. Dong, "An improved particle swarm optimizer for parametric optimization of flexible satellite controller," *Applied Mathematics and Computation*, vol. 217, no. 21, pp. 8512–8521, 2011.

[34] J.-S. Wang and J.-D. Song, "Function optimization and parameter performance analysis based on gravitation search algorithm," *Algorithms*, vol. 9, no. 1, p. 3, 2015.